Biological Systems Engineering: Papers and Publications

Biological Systems Engineering

5-2019

Field evidence of a natural capillary barrier in a gravel alluvial aquifer

Todd Halihan
Oklahoma State University, todd.halihan@okstate.edu

Ronald B. Miller
Oklahoma State University

David Correll
Oklahoma State University

Derek M. Heeren
University of Nebraska-Lincoln, derek.heeren@unl.edu

Garey A. Fox
North Carolina State University, gafox2@ncsu.edu

Follow this and additional works at: https://digitalcommons.unl.edu/biosysengfacpub

Part of the Bioresource and Agricultural Engineering Commons, and the Civil and Environmental Engineering Commons

Core Ideas

- A tracer test in a gravel aquifer detected a natural capillary barrier.
- Electrical resistivity data combined with well data found two separate vadose zone flow paths.
- Phosphorus transport is limited, as it needs to migrate through soil before gravel.

Field Evidence of a Natural Capillary Barrier in a Gravel Alluvial Aquifer

Todd Halihan,* Ronald B. Miller, David Correll, Derek M. Heeren, and Garey A. Fox

Ozark streams commonly feature "composite" floodplains, in which the vadose zone consists of silt or silt loam soils ($\sim$1 m thick) overlying gravel subsoil. Previous work has shown that preferential flow paths can exist within the gravel subsoil, which can conduct water and P at rates exceeding the sorption capacity of the gravel. At a site on Barren Fork Creek, a 1- by 1-m infiltration plot was constructed and an infiltration experiment was performed using sequentially introduced solutes including P (the constituent of regulatory interest), Rhodamine-WT (Rh-WT, a visual tracer), and Cl$^-$ (an electrical tracer). The solute transport was measured with monitoring wells (MWs) placed 1 m from the plot boundary and 5 m down the groundwater flow gradient using an electrical resistivity imaging (ERI) array. The ERI method utilized differences between a pre-infiltration background image and subsequent temporal images taken during the test to quantify changes induced by the tracers. The infiltration test maintained a steady-state flow rate of 4.5 L min^{-1} for 84.75 h. Electrical resistivity imaging data showed significant changes in resistivity induced by the tracers within the soil vadose zone under the plot but no similar changes within the gravel, indicating that the interface was acting as a capillary barrier. Electrical resistivity images 5 m away from the plot showed tracer breakthrough into the gravel in areas not sampled by the MWs. Solute detection was limited in MWs, indicating that MWs could not adequately monitor movement below the capillary barrier because it controlled migration of solute to the heterogeneous phreatic zone.

Abbreviations: ERI, electrical resistivity imaging; MW, monitoring well; Rh-WT, Rhodamine-WT; SRP, soluble reactive phosphorus; TP, total phosphorus.

T. Halihan, School of Geology, Oklahoma State Univ., Stillwater, OK 74078; R.B. Miller and D. Correll, Environmental Sciences Program, Oklahoma State Univ., Stillwater, OK 74078; D.M. Heeren, Biological Systems Engineering Dep., Univ. of Nebraska, Lincoln, NE 68583; G.A. Fox, Dep. of Biological and Agricultural Engineering, North Carolina State Univ., Raleigh, NC 27695. *Corresponding author (todd.halihan@okstate.edu).

Heterogeneity is a common element in natural systems, including fluvial systems where the interaction of erosive and depositional forces creates complex features composed of many different textures and geometries (Miller et al., 2015). Floodplains are fluvial features that are both economically and environmentally important (Opperman et al., 2009) because of their positioning at the interface of the land surface and the hydrologic system. Materials and pollutants on the floodplain surface have relatively short flow paths both across the floodplain surface and through the floodplain vadose zone to reach the stream water. In these floodplain environments, the heterogeneity of texture and layering within floodplains can create complex flow paths in the vadose zone (Hillel, 1987), making it difficult to predict the transport of infiltrating constituents.

Heterogeneity is high in composite floodplains (Fox et al., 2011), where fine-textured cohesive soil overlies non-cohesive gravel. This heterogeneity is partly responsible for the high erosion rates often seen in the streambanks of these floodplains (Thorne and Tovey, 1981; Midgley et al., 2012), driven by the high erodibility of the unconsolidated gravel during extreme flood events. In a study also related to the heterogeneity of composite floodplains, Fuchs et al. (2009) found that water flow occurred at a rate high enough to prevent P from sorbing to the substrate within a preferential flow path in the gravel vadose zone. Phosphorus is a significant contaminant in freshwater streams and lakes, primarily because of its role in eutrophication (Moore and Edwards, 2007). The chemistry of P in the natural environment is complex, but because of its tendency to sorb to clay and organic material, it is generally thought of as a chemical species with limited subsurface

mobility (Daniel et al., 1998). However, where the possibility of rapid P transport through gravel exists (Fuchs et al., 2009), the fate of P moving through the thin cohesive alluvial soils of composite floodplains must be explored.

When the contrast between soil textures in a heterogeneous environment is high enough, the difference in pore sizes can produce a capillary barrier, which can affect the movement of water within the vadose zone (Corey, 1994). The capacity for capillary barriers to retard and deflect the infiltration of water through the vadose zone has been detected in natural soils (Heilig et al., 2003) and exploited in the engineering of landfill caps (Stormont, 1996; Ho and Webb, 1998; Khire et al., 2000). Stormont (1996) showed that engineered capillary barriers were capable of diverting the breakthrough from fine to coarser soils several meters laterally from the point of infiltration. The presence of a strong natural texture contrast, such as in a composite alluvial floodplain, may complicate detecting and predicting the movement of water and measuring dissolved P or other constituents as water infiltrates from the floodplain surface.

Field studies involving the detection of the movement of water and tracers from the land surface to the water table can be problematic to design. The traditional water and tracer characterization method, namely discreet sampling over time from MWs, works very well if the infiltration occurs predictably, for example vertically through the vadose zone to the saturated zone. In that case, the MWs can be placed near the infiltration source with a reasonable chance to intercept the tracer. However, MWs have a very limited detection area and may not be effective if the target water or tracer preferentially moves meters away through the vadose zone along a capillary barrier. Also, MWs can effectively sample only from the saturated zone, even if the well screen extends into the vadose zone. The well bore presents a capillary barrier relative to fine-textured soil and the well may miss tracer movement or moisture changes occurring above the saturated zone. Tensiometers are effective at detecting changes in vadose zone soil moisture but, like MWs, are limited in detection area, and their use is problematic in gravelly soils with large pore spaces. Capturing solutes with MWs can be difficult under heterogeneous anisotropic conditions. Researchers such as Garabedian et al. (1991), LeBlanc et al. (1991), and Werth et al. (2010) have traditionally used two methods to test transport analysis: (i) fluid flow through porous media is traced through indirect measurements of a conservative tracer or to monitor chemical transport, and (ii) a reactive solute is used and changes in chemical concentrations are measured to test the amount of chemical retardation of flow. An alternative approach to these methods is to conduct an electrical tracer test using electrical resistivity equipment.

Geophysical methods are nondestructive compared with many vadose zone sampling techniques and are sensitive to differences or changes in soil moisture in the vadose zone (Cassiani et al., 2006). A multitude of geophysical techniques exist to detect soil moisture changes. In contrast to ground-penetrating radar, electrical resistivity imaging (ERI) can effectively and reliably image both fine-grained cohesive soils and coarse gravel. Because ERI utilizes an array of electrodes, it can effectively sample a much larger area than a monitoring well (Halihan et al., 2005). Electrical resistivity imaging technologies have been used to characterize contaminated sites, identify resistivity differences in gravels, and observe moisture content changes in the vadose zone setting. Beresnev et al. (2002) used ERI integrated with confirmation drilling for gravel aggregate prospecting and observed that gravel with low amounts of fine materials had significantly higher resistivity than the surrounding geologic strata. Arora and Ahmed (2011) used time-lapse ERI to image wetting fronts in the vadose zone as an aid in estimating aquifer recharge from rainfall. Halihan et al. (2012) used ERI to identify solvent-related geophysical anomalies at a release site. Sima (2008) used ERI to demonstrate that a bulk saline tracer fluid can be time lapse imaged at the Barren Fork Creek site. Miller et al. (2014) used ERI to map the alluvial floodplain at the Barren Fork Creek site and suggested that areas of high resistivity might correlate with areas containing preferential flow paths or the potential to transport P at a high velocity into the shallow groundwater system. In a complex system where traditional methods have failed, this technology must be advanced by integrating hydrogeophysical data with traditional site characterization methods to better understand flow and transport.

The Barren Fork Creek site is well characterized by previous research and has a shallow gravel aquifer available for evaluating flow and transport mechanisms. Furthermore, Barren Fork Creek is located in the Ozark ecoregion in which poultry production is an important economic activity, and preserving surface water quality is an important goal (Soerens et al., 2003; Andrews et al., 2009). A review of federal regulation and litigation in the Ozark ecoregion related to P was presented by Freiberger (2014). The surface application of poultry litter, which as an agricultural amendment is relatively high in P, has been implicated as a nonpoint P source (Moore and Edwards, 2007). We hypothesize that by conducting a tracer test at a well characterized site while regularly sampling large screened MWs, along with utilizing a temporal resistivity imaging technique and dynamic well placement during the tracer test (placing the well after evaluating geophysical data), we should be able to determine the velocity, direction, and retardation of the tracer solution. The objectives of this experiment were to run a tracer test with electrically variable fluids in a gravel aquifer, evaluate geophysical data to determine whether the nonconservative solutes change the bulk electrical properties as they are retarded, and evaluate the results to determine whether the protocols used are effective at quantifying flow and transport in a heterogeneous anisotropic medium. The expectation of the experiment was that the heterogeneity of the medium would be the controlling variable on transport detection and evaluation; the results indicated that the transient capillary barrier effects ended up being the stronger control on flow location and duration. While still meeting the objective of tracking the fluids and solutes, this effect altered procedures during the experiment to track fluid moving along the capillary barrier instead of tracking only through a well-characterized gravel.

To better understand flow through heterogeneous anisotropic media, greater data density with higher resolution is needed to capture meter-scale flow features that are unique because most hydrologic studies focus on 1-km flow features. Riparian zone agroecosystem management principles, such as the practice of land application of P-laden chicken litter, could be changed in response to the findings of this research. By combining the two-dimensional high-resolution temporal ERI data with point data from wells and modifying the sampling domain during the experiment, tracking tracer flow and transport in heterogeneous media becomes more of a possibility. This may alleviate the problem of not detecting tracers with wells and pondering which conceptual model is appropriate for the lost tracers.

Site Description

The Ozark ecoregion is located in northeastern Oklahoma, northwestern Arkansas, southeastern Kansas, and southwestern Missouri. The Barren Fork Creek site is located in the Oklahoma portion of the Ozark ecoregion, 11.3 km east of Tahlequah, OK (Fig. 1). The average precipitation near the Barren Fork Creek site at the Tahlequah Mesonet weather station is 112 cm (44 inches) (Oklahoma Mesonet, 2013). The Barren Fork Creek has an average stream discharge rate of 6.6 $m^3\ s^{-1}$ (320 cfs) at the USGS gauging station at Eldon Bridge (USGS, 2013).

The site was selected because both soils and gravels are present (Fig. 2) as determined by previous geophysical work by Heeren et al. (2011). The ideal site should enable water to flow fast enough to monitor solutes without a high flow velocity exceeding the capability of providing a sufficient input tracer solution volume. An elevated level of heterogeneity was previously demonstrated at the site due to the high number of preferential flow pathways. This
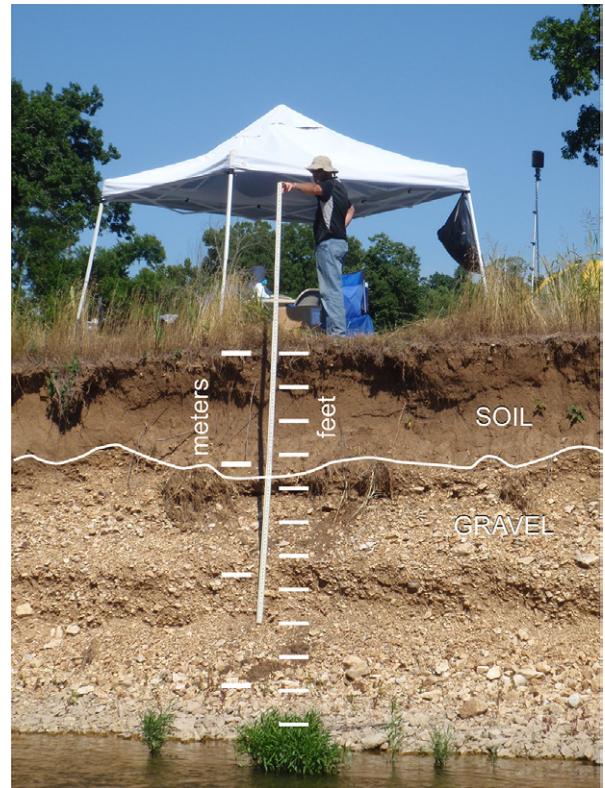

Fig. 2. Soil profile at the tracer infiltration site. The cut bank of the Barren Fork Creek is immediately adjacent to the tracer experiment site. The subsurface consists of approximately 1 m of silt loam soil underlain by chert gravel. The alluvial water table is approximately 3.25 m below the ground surface.

site has been well characterized in previous research (e.g., Fox et al., 2011). The soil at the Barren Fork Creek site is silt loam, with the soil series predominately Razort gravelly loam (a fine-loamy, mixed,
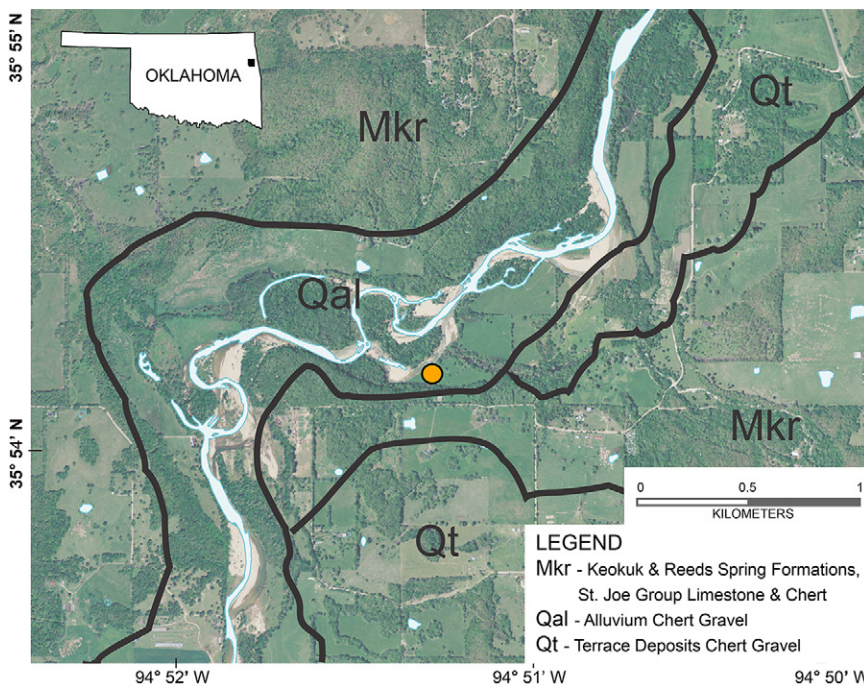

Fig. 1. Location and geology at the Barren Fork Creek test site. Aerial image from National Agricultural Imagery Program (2010).

active, mesic Mollic Hapludalf) and Elsah gravelly loam (a loamy-skeletal, mixed, superactive, nonacid, mesic Typic Udifluvent) (Miller et al., 2014). Examination of soil cores from the infiltration plot showed that the soil profile in that location was silt loam with some gravel, with a distinct change at the 1-m depth to coarse chert gravel. Within the gravel, silt loam particles occurred less frequently with increasing depth.

The bedrock geology at the Barren Fork Creek site is primarily Mississippian-aged Keokuk and Reed's Spring formations. Limestone, chert, and lesser amounts of siltstone, shale, and sandstone comprise the uplands above and upstream of the site and are the parent rock for the local alluvium, which is predominantly chert gravel and cobbles. Within the stream valley, the chert gravel beds are variously outcropped (within the active channel) and buried by a soil mantle (within the floodplain).

Floodplain gravels with high saturated hydraulic conductivity (K_{sat}) values are an important element of the hydrogeology of this site. A direct-push constant-head permeameter (Miller et al., 2011) was used to measure vadose zone hydraulic conductivities of up to 400 m d^{-1} at the Barren Fork Creek site, resulting in a positive correlation between apparent resistivity and hydraulic conductivity (Miller et al., 2014). Fuchs et al. (2009) found that those vadose zone gravel transport rates were sufficiently high to prevent sorption of P at the meter scale. The local geology is well suited for this tracer test because of the heterogeneous anisotropic conditions and high K_{sat} gravels. The site has shallow groundwater, which can be encountered at 3 m from the surface. The shallow groundwater at this site interacts with the adjacent surface water, which is significant for the P transport potential because the interaction between the surface and the groundwater is a pathway for contaminant transport. Heeren et al. (2011) described how the water table fluctuated and was dependent on the stream stage, where a peak high-flow event indicated that water was leaving the Barren Fork Creek and entering the gravel aquifer system, but at normal stage, water was leaving the aquifer and entering the stream in a south–southwest direction away from the infiltration site. The potentiometric surface gradient of the shallow groundwater is greatest during high-flow stream stages in the Barren Fork Creek but less when the stream stage is at a low flow rate, which indicates that the system is variable in the flow direction as mentioned above but also that the magnitude of change is dependent on the stream stage (Heeren et al., 2014a).

Methods
Infiltration Test Modes

A 1-m^2 portable and reusable infiltration plot was constructed to provide a constant head during the infiltration test (Fig. 3 and 4; Heeren et al., 2014b). The plot border was constructed with vinyl hose (inside diameter = 15.24 cm [6 inches]) connected to steel right-angle tubing with heavy-duty hose clamps. Once a suitable area for the infiltration plot was selected, the border of the plot was prepared by scraping the vegetation from the floodplain surface directly

beneath the hose, and a seal was created between the prepared soil and hose by applying hydrated bentonite clay. The hose assembly was then filled with water to give the plot edges rigidity and mass (Fig. 4). It is important to note that the area directly beneath the plot border
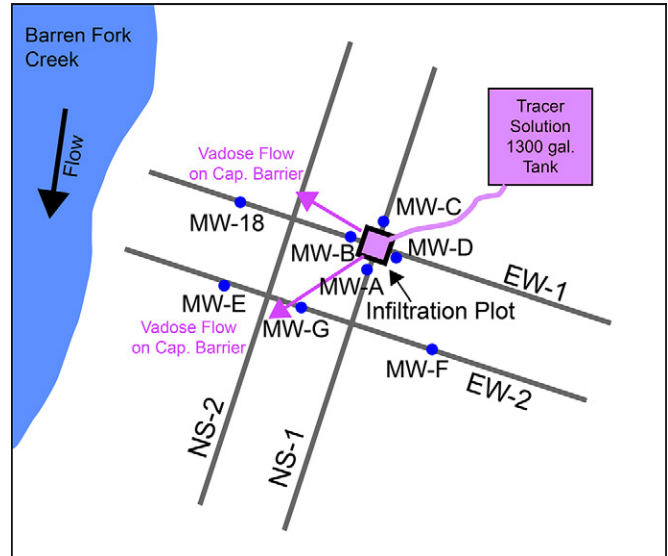

Fig. 3. Configuration of infiltration plot, monitoring wells (MWs), and resistivity lines at the Barren Fork Creek site. Wells MW-A, -B, -C, and -D were 1 m from the plot center and MW-E and -F were placed on a line 5.5 m from the plot center, while MW-18, located 13 m from the infiltration plot, was established as part of a previous research project, and MW-G was placed after infiltration commenced based on geophysical data. Purple arrows note observed directions of change in electrical properties on distant lines. The electrical resistivity imaging lines were arranged in parallel pairs, with one line (EW-1) through the center of the plot and the other (EW-2) separated by 5.5 m. The alluvial groundwater flow direction was approximately parallel to the stream flow direction.
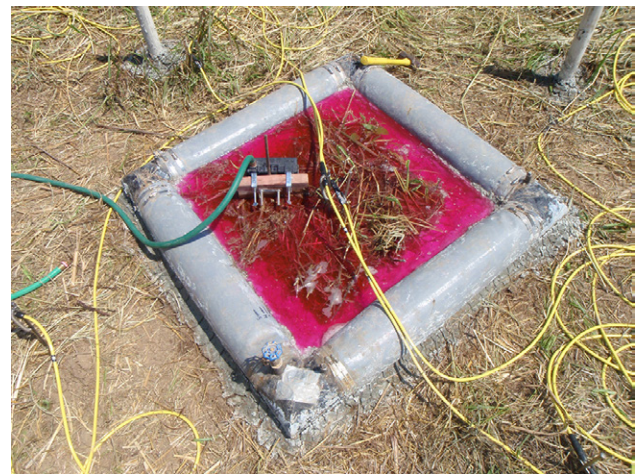

Fig. 4. Infiltration plot, monitoring wells, and resistivity electrodes for longitudinal and transverse lines in the center of the plot as well as associated cabling. The background contains wells MW-A and MW-D. The infiltration inlet hose (green) and float valve used to maintain a constant level within the infiltration pond are also shown. Rhodamine-WT tracer is present in the infiltration fluid. Also notable is the presence of undisturbed vegetation within the pond and the absence of leakage under the pond edges.

was the only portion of the infiltration plot disturbed; the interior of the plot remained undisturbed and was assumed to represent the infiltration characteristics of the floodplain surface.

Water (and solutes) was introduced into the plot from a 4920-L (1300-gallon) agricultural water supply tank with volumetric graduations, using gravity flow through a hose connected to an agricultural tank float regulator positioned inside the plot. The tank float regulator was adjusted to maintain a water level within the plot of 7 cm (2.75 inches). A small auxiliary tank was utilized to provide inflow during the mixing of tracer solutions in the large tank. The water used during the test, including for preparing tracer solutions, was native water from Barren Fork Creek.

Solutions were mixed in the large tank using a closed-loop flow-through system powered by a high flow volume, gasoline-powered water pump. Three solutes were added to achieve different tracing objectives. The primary tracer was P, as it was of interest for transport properties through the gravel. However, it was the hardest to detect in the field either visually or geophysically, so other solutes were added afterward as location tracers so field adjustments could be made to try to catch flow paths in the heterogeneous phreatic zone. Rhodamine-WT was added as a visual tracer that could be seen in wells by color to determine direction prior to any arrival of P. Finally Cl$^-$ tracer was added to provide an increased geophysical contrast in the fluid if the changes in soil moisture were difficult to detect with ERI. The tracers were separated in this manner for two additional reasons. First, in order to have sufficient time for the P to transport through the soil column and into the gravel aquifer, sufficient time was available to wait for other tracers to be added. Second, if a geophysical signature from the tracers occurred unexpectedly, it would be clear which constituent was responsible.

Solutes were prepared to the following specifications: P was prepared by mixing liquid H$_3$PO$_4$ to a target concentration of 10 mg L^{-1}; Rh-WT was mixed to a target concentration of 10 mg L^{-1}; and Cl$^-$ tracer was prepared by mixing solid granular KCl with stream water to a target concentration of 100 mg L^{-1}. Once a solute was started, it was continued until the end of the infiltration test, with solutes cumulatively added in the following order: unaltered stream water, P, Rh-WT, and Cl$^-$ tracer.

Monitoring Well Procedures

All monitoring wells (MWs) utilized during the infiltration experiment were installed using a Geoprobe TMP 6200 direct-push rig (Geoprobe, Inc.). The casing used on all wells was 5-cm (2-inch) diameter polyvinyl chloride (PVC), with a factory slotted screen. Wells were placed to a total depth of 4.9 m (16 ft) below ground surface (BGS), with a 3.05-m (10-ft) screen section from 4.9 to 1.8 m (16–6 ft) BGS, and then solid PVC casing from 1.8 m BGS to 0.3 m above the surface (6 ft BGS to 1 ft above). Coarse sand was used as a filter pack in the annular space from 4.9 to 0.6 m (16–2 ft) BGS, and a bentonite seal was placed in the annular space from the surface to 0.6 m (2 ft) BGS to prevent surface waters from entering the well bore.

The MWs were placed in the following configuration once the plot location was established: four MWs (MW-A, MW-B, MW-C, and MW-D placed clockwise from the southwest edge of the infiltration plot) were constructed 0.5 m away from each of the four sides of the plot (Fig. 3). Additionally, three MWs (MW-E, MW-F, and MW-G) were installed 5.0 m downgradient in the presumed groundwater flow direction from the injection plot. These wells are located along an ERI line (EW-2). (Monitoring Well G was constructed during the infiltration experiment to attempt to intercept fluid movement detected by ERI. The location was selected by choosing the strongest fluid signal observed above background in the images after the first two images were available for the site by processing data in the field.) Several existing MWs were utilized in the infiltration experiment; MW-18 was located on the EW-1 ERI line west of the plot; MW-22 was located approximately 10 m to the northwest of the infiltration plot; and MW-33 was located on the floodplain approximately 35 m east of the plot and was used for background samples during the experiment. All of these wells had similar construction, except the total depth was ∼6 m for the existing MWs.

During well construction, soil cores were collected at MW-A and MW-C using a Geoprobe dual-tube sampler. After the infiltration test, a core was collected from the center of the plot. This provided a total of two cores prior to the experiment and one core exposed to the full solute suite after the experiment. The MW-A and MW-C cores were examined in the field to determine the depth of the gravel–soil interface below the infiltration plot. The cores were transported to the laboratory for inspection, and samples from the cohesive soil portion of the cores were selected and dried. Those samples were further analyzed for particle size distribution, bulk density, and water-soluble and total P.

Water levels in the infiltration plot and supply tanks were monitored during the infiltration experiment with HOBO U20 Water Level dataloggers. The dataloggers were synchronized to collect pressure and temperature data every minute. A datalogger was installed on the infiltration plot surface to monitor the water level in the plot during the experiment. An additional datalogger was placed in the supply tank to monitor the change in water level with outflow, which allowed a calculation of the infiltration rate and the total volume infiltrated.

Water samples were obtained from each MW and from the Barren Fork Creek before and during the infiltration experiment, with the background water samples representing a chemical baseline at all water wells and the creek before infiltration began. The MWs were sampled approximately every 4 h during the experiment. Prewashed 500- and 250-mL Nalgene sample bottles were used to collect water samples. The sample bottles were rinsed with sample fluid three times before a sample was collected to eliminate any contamination from the sample bottles. The peristaltic pump used to pump water samples from the well was rinsed with deionized water previous to each sample collection to prevent cross-contamination. Samples for soluble reactive P (SRP) analysis were vacuum filtered to remove particulates and acidified with H$_2$SO$_4$ while in

the field. Samples to be used for determining total P (TP), Rh-WT, and Cl⁻ tracer concentrations were not filtered. All samples were labeled with the MW name, date, and time sampled and stored in coolers packed with ice while awaiting transport to the laboratory for analysis.

The SRP was determined colorimetrically with the modified ascorbic acid method (USEPA, 1971; Murphy and Riley, 1962) with a spectrophotometer (DU 720, Beckman Coulter, minimum detection limit of 0.002 mg L⁻¹). Autoclave persulfate digestions (APHA, 1999) were performed on unfiltered TP samples to dissolve any particulate or organic P. The TP (minimum detection limit of 0.01 mg L⁻¹) was then determined colorimetrically by the modified ascorbic acid method. The Rh-WT samples were analyzed with a Trilogy laboratory fluorometer (Turner Designs, minimum detection limit of 0.01 mg L⁻¹). The Cl⁻ concentrations were determined by ion chromatography (minimum detection limit of 0.16 mg L⁻¹).

Resistivity Monitoring

Four resistivity lines were positioned in pairs at right angles over the infiltration plot, with two crossing in a generally east–west trend (EW-1 and EW-2) and two crossing in a general north–south trend (NS-1 and NS-2), with each pair (e.g., EW-1 and EW-2) being run simultaneously (Fig. 3). Each resistivity line utilized 28 stainless steel electrodes with a spacing interval of 1 m, giving each line a total length of 27 m, a depth of investigation of 5.5 m, and image resolution of 0.5 m. The EW line pair was positioned normal to, and the NS line pair parallel to, the creek bank. One of each pair of lines (EW-1 and NS-1) crossed through the infiltration plot to monitor the electrical changes near and below the infiltration site, while the remainder of each pair (EW-2 and NW-2) was located 5.5 m downgradient (east and south, respectively, measured from the plot center) along the presumed direction of groundwater flow (Heeren et al., 2014a). The center of the plot was located near 14 m on EW-1 and 9 m on NS-1.

Resistivity data were collected using a SuperSting R8/IP Earth resistivity meter (Advanced GeoSciences) and were topographically corrected with elevation data collected with a laser level (±0.5 cm) at each electrode during setup. An Oklahoma State University ERI method of acquisition and inversion (Halihan and Fenstemaker [2004], commercially applied as GeoTrax Surveys, aestusllc.com) was utilized to acquire and process the data, providing methods parallel to those utilized for equivalent field and laboratory research (Halihan et al., 2005, 2017; Acharya et al., 2017). These resistivity acquisition and data inversion techniques were developed to evaluate resistive subsurface signatures and have been applied to more than 200 research and commercial sites (Halihan et al., 2005, 2012; Miller et al., 2014). The method utilizes a least-squares optimization L₂ norm inversion (deGroot-Hedlin and Constable, 1990). Previous work compared the technique to common resistivity approaches for resistivity data (Halihan et al., 2005; Miller et al., 2014) and temporal resistivity data (Halihan et al., 2011, 2017). The technique provides improved stability in

temporal data when compared with standard methods. The grid for the inversion was a regular block centered grid with a resolution of half the electrode spacing. The inverted resistivity data were contoured using Golden Software's Surfer software for visualization purposes. Terms in the literature for electrical datasets vary. For this study, the inverted bulk resistivity values of the acquired surface resistivity data are termed *resistivity* in an attempt to avoid confusion with fluid conductivity data. The contoured, inverted resistivity model datasets are termed *images*. The temporal data refer to an increase in conductivity because the tracer causes positive changes in conductivity when detected.

The resistivity data were acquired to monitor changes in the electrical properties of the subsurface induced by the infiltration of water and solutes. To accomplish this, a differencing inversion was performed, modeling the change between temporal images. Specifically, two "background" images were acquired independently for each line prior to the start of infiltration. These images were differenced and the resulting image, representing no effects from infiltration, was used in the determination of the change induced by subsequent water and solute infiltrations. It was assumed that infiltration of water and solute would generally reduce the bulk resistivity of the subsurface, which is equivalent to increasing the bulk conductivity. To portray infiltration-induced changes as positive, the differenced ERI images are scaled to portray changes in conductivity, with positive values indicating greater conductivity (lower resistivity) with time. Including the background images, ERI data for differencing were collected before, soon after, and long after starting infiltration and each subsequent solute, with the time interval between images being approximately 6 h.

◆ Results

Infiltration Plot Data

The water infiltration began at 4:30 PM on 6 June 2012 and continued for the next 84.75 h. The flow rate of the plot into the subsurface was 4.47 L min⁻¹ (1.18 gpm) with 23,000 L (6000 gal) of total infiltration. Infiltration of P began at 8:10 PM on 7 June 2012, Rh-WT began infiltration at 2:55 PM on 8 June 2012, and Cl⁻ tracer began at 11:15 AM on 9 June 2012 (Fig. 5). Head within the infiltration plot averaged 6.7 cm (2.75 inches) during the infiltration test. The test ended when the tracer solution tank was allowed to run dry at 5:15 AM on 10 June 2012. Samples taken directly from the 1- by 1-m plot averaged 8.3 mg L⁻¹ SRP and 8.5 mg L⁻¹ TP, 61.6 mg L⁻¹ Cl⁻, and 7.3 mg L⁻¹ Rh-WT. The fluid electrical conductivity in the infiltration plot increased from 117 to 225 μS cm⁻¹ when the KCl solution was initiated.

Well Data

A number of samples were drawn from Barren Fork Creek, the infiltration plot, and each MW beginning with the initial stream water infiltration and ending at the termination of the experiment, with a total of 12 samples from each MW (except
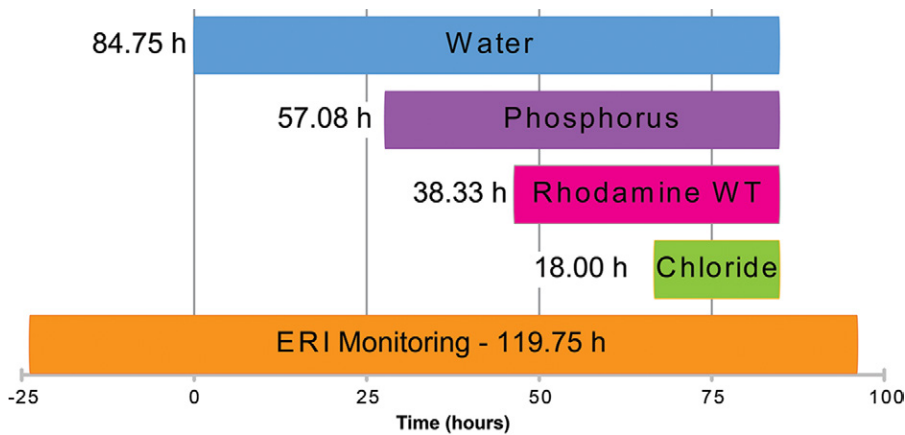
Fig. 5. The timing of electrical resistivity imaging monitoring (orange bar) and the introduction of water, P, Rhodamine-WT, and KCl into the infiltration pond. The bottom axis shows experiment timing, with 0 at the start of water infiltration. The total duration of each injection is shown, indicating that the tracers were introduced sequentially then continued until the end of the experiment.

MW-G, where six were drawn), nine plot samples, and six stream samples. The baseline concentrations were calculated from the samples before the tracer initiation and were very low and comparable to the stream samples. Baseline SRP concentrations were approximately 0.02 mg L^{-1}. Due to the occasional inclusion of sediment in the groundwater samples during sample collection with the peristaltic pump, the practical detection limit for TP was 0.4 mg L^{-1}, and pre-introduction concentrations in the stream, plot, and MWs were all well below this threshold (approximately 0.1 mg L^{-1}). Due to the matrix of the natural water (compared with distilled water), the practical detection limit for Rh-WT was 0.01 mg L^{-1}. Rhodamine-WT was not detected in baseline samples (approximately 0.003 mg L^{-1}), as Rh-WT was not expected to occur naturally. Pre-introduction Cl$^-$ concentrations in the stream, plot, and MWs were 4 to 6 mg L^{-1}.

In general, after solutes were introduced to the infiltration plot, concentrations from samples drawn from the plot approached the target solute concentration. In contrast, solute concentrations in samples from the MWs were much lower, and in many cases were below detection. In particular, no MW SRP samples were significantly above the baseline SRP. Only 1 TP (MW-E) was significantly above the detection limit, probably an anomalous sample (SRP = 0.003 mg L^{-1}, TP = 7.39 mg L^{-1}). Average post-infiltration Rh-WT concentrations were above the detection limit in MW-A (0.56 mg L^{-1}) and MW-D (0.016 mg L^{-1}). Average post-infiltration Cl$^-$ concentrations were increased above the baseline only in MW-A (11.6 mg L^{-1}) (Fig. 6). The detection of Rh-WT but not Cl$^-$ in MW-D is probably because the injection level of Rh-WT was three orders of magnitude above the Rh-WT minimum detection limit, allowing detection even after significant dilution. No other wells, including MW-G, which was dynamically sited in a location where the vadose zone had initial changes in bulk resistivity, had detections above background for any of the tracers.

Integrated geophysical data and well data indicate that the tracers in the wells, where detected, probably migrated through the soil and along the capillary barrier to the well location instead of downward and through the gravel aquifer. Using the well locations where solute detection occurred, the tracer velocity for Cl$^-$ is estimated in a range of 1.6 to 19.7 × 10^{-5} m s^{-1}. For P, the velocity estimate is a range of 2.4 to 9.0 × 10^{-5} m s^{-1}. These velocity values assume a straight-line path to the well and vertical movement to the screen to determine the distance. The travel time was between the initial addition of a tracer and the first detection of a solute. The retardation of P is estimated between 1.5 and 2.2.

Geophysical Results

During the first 26 h of the experiment, only creek water was infiltrated into the plot, and each line orientation was taken back-to-back for that period but with some time lag in between starting each resistivity profile; about a 3-h time separation was achieved. This resulted in an approximately 6-h sampling interval for each ERI dataset. The ERI lines EW-1 and EW-2 increased resistance during contact resistance tests compared with NS-1 and NS-2, but all were below 2000 Ω in the soil. No fluids were required to increase contact with the soil. A total of eight ERI images were collected during the experiment for each pair, including two images collected before the initiation of water infiltration and images collected before and after the introduction of each new solute. Total root mean squared error for the resistivity inversions was between 3.1 and 9.1%, with an average of 6% root mean squared error. For the resistivity differencing, the errors were between 0.7 and 7.0%, with an average of 2.7% error. The sensitivity was good throughout the image, indicating that the image and inversion quality was very good. The initial (pre-tracer) images for each pair were obtained about 4 h apart, and differencing of those images yielded matrix changes of inverted resistivity of ≤2%; therefore, only differences >2% were regarded as significant. Subsequent differencing of ERI images obtained before and after the initiation of water infiltration and each subsequent solute produced significant differences in images only after the initiation of water infiltration and Cl$^-$ tracer; the P and Rh-WT had only slight effects on the electrical nature of the subsurface.

The ERI images from the addition of stream water and the Cl$^-$ tracer along NS-1 (Fig. 7A), which portray a subsurface plane through the infiltration plot, showed an increase in conductivity (decrease in bulk resistivity) in the fine-grained cohesive soil directly below the plot but not extending across the texture interface into the gravel. During both times, resistivity differences were
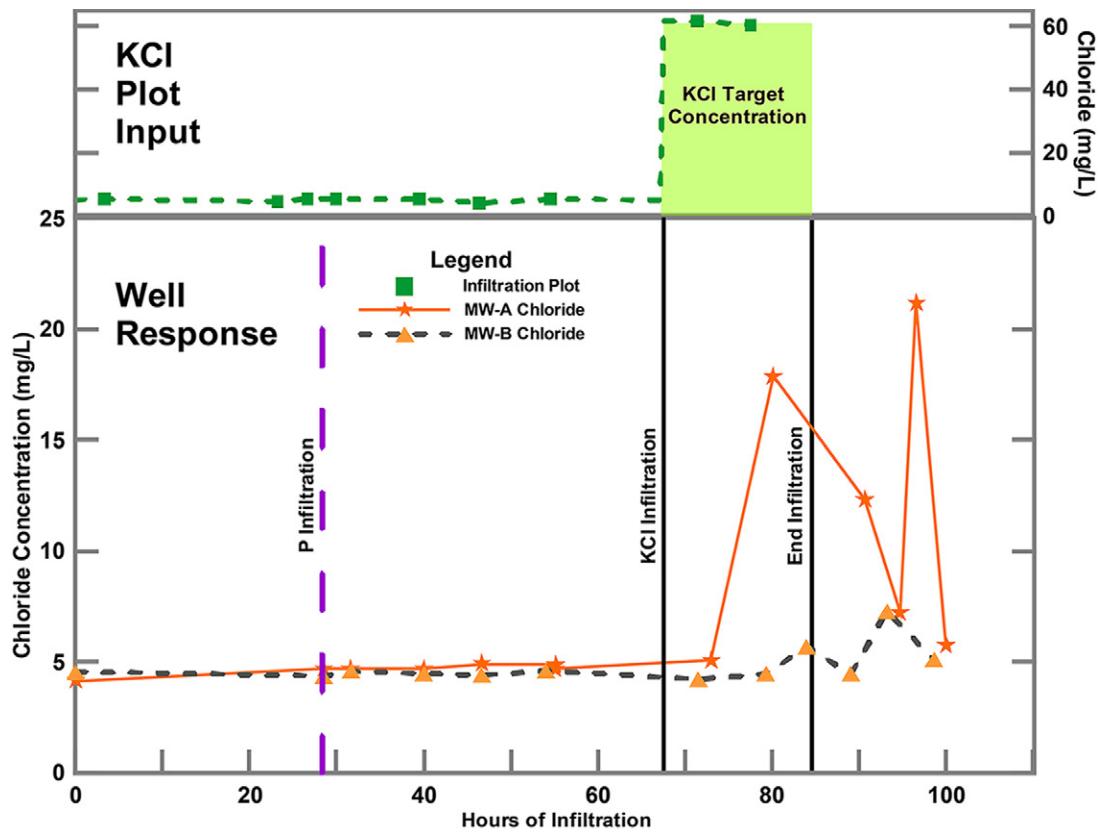
Fig. 6. The change in concentration of Cl⁻ within the infiltration plot and nearby monitoring wells (MWs) following the addition of the Cl⁻ tracer to the infiltration plot. Plot Cl⁻ concentration was ∼60 mg L⁻¹. Well MW-A (located 1 m south of the plot) shows an increased Cl⁻ level about 12 h after the Cl⁻ tracer was added, while MW-B (located 1 m west of plot) shows concentrations slightly elevated above background level after about 25 h. No other MW had an increased level of Cl⁻.

above background, with an increase in conductivity of approximately 30% from soil wetting and an additional increase of 20% from the addition of the Cl⁻ tracer (Fig. 8). The effect of this capillary barrier is shown in Fig. 8, which displays the net change from the baseline with time for a vertical series of ERI data nodes from NS-1 located within the plot. The data show a constant increase in electrical conductivity (decrease in resistivity) with the onset of water infiltration to a maximum increase of about 32%. These data also show that while the addition of the P and Rh-WT had no effect on the change in bulk resistivity, the Cl⁻ tracer had a significant effect on resistivity. Most notably, the bulk resistivity did not change below the gravel–soil interface, which shows that the water and subsequent tracers were not crossing the capillary barrier below the plot, even after >80 h of infiltration.

The region of conductivity increase in NS-1 also intersects the well bore of MW-A (Fig. 7), where it passes through the soil layer. This may mean that the Cl⁻ increase in MW-A could be due to small amounts of Cl⁻ tracer entering the well bore in the vadose zone and then flowing down the well casing to the water table, locally increasing the Cl⁻ concentration within the well bore.

The ERI images offset from the plot (NS-2 and EW-2) each have areas with increases in conductivity (EW-2 shown in Fig. 7B). These increases can only be due to water and Cl⁻ tracer infiltration, implying that flow from the plot moved preferentially through

the vadose zone in these directions (Fig. 3). These conductivity increases extend below the gravel–soil interface, implying that breakthrough across the capillary barrier from the cohesive soil into the gravel vadose zone occurred somewhere along these flow paths. A plot of the change from the baseline at a vertical resistivity node transect located on image EW-2 near MW-G shows that the increase in conductivity occurred below the gravel–soil interface, and the upper soil layer shows a reduction in conductivity, probably due to the progressive soil drying during the experiment (Fig. 9).

Discussion

If infiltration was vertical and continuous between the infiltration plot and the water table, we would expect that solute concentrations would be highest in at least one of the MWs closest to the plot (MW-A, MW-B, MW-C, or MW-D) and that solute concentrations from those MWs would approach the concentration from the plot. Furthermore, it would follow that MWs farther from the plot and downgradient with respect to the water table (MW-E, MW-F, and MW-G) would be more influenced by mixing as the tracer plume moved downgradient and therefore concentrations from those wells would show somewhat reduced solute concentrations. The solutes expected to most closely approach plot concentration in MW samples were the Rh-WT and Cl⁻ tracers,
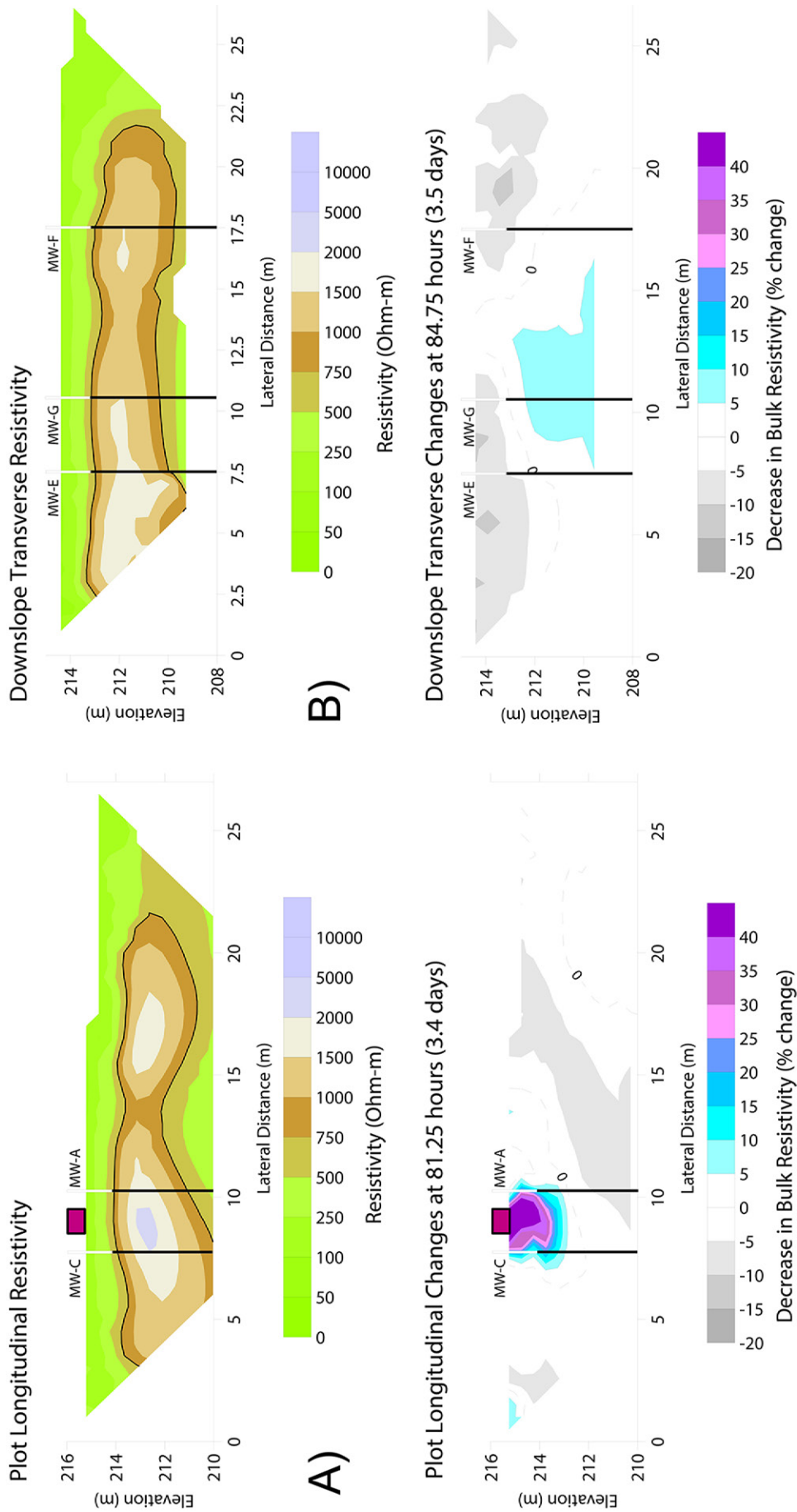
Fig. 7. Initial bulk resistivity images prior to introduction of tracer fluids (upper) and images showing maximum difference for temporal electrical resistivity imaging (ERI) images (lower) and the location of monitoring wells: (A) NS-1 ERI line through plot, where resistivity change in the vadose zone in NS-1 temporal data between 8 and 12 m laterally is due to water moving through the gravel layer, and the large resistivity difference in the soil zone coupled with the absence of difference in the gravel vadose zone below the infiltration plot in the temporal image indicates that the texture contrast acts as a capillary barrier; and (B) EW-2 ERI line offset from plot. Increase in conductance between 8 and 12 m laterally in the gravel zone is interpreted as breakthrough of tracer through the capillary barrier. Screened intervals of monitoring wells are shown in black.
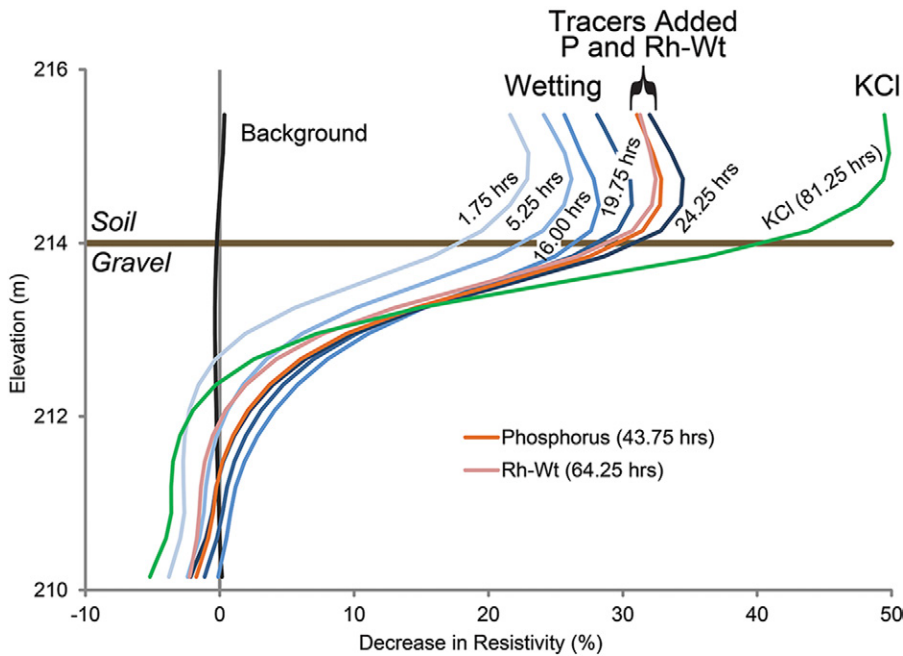
Fig. 8. Plot of the vertical resistivity changes with elevation over time at the location of the infiltration plot from electrical resistivity imaging line NS-1. The bottom axis is the decrease in resistivity, and the lines are the difference between background and the image taken at the noted time interval. The background (black line) is the difference between two images taken before infiltration was initiated. Initial and subsequent wetting of the plot (light blue to dark blue lines, 1.75–19.75 h after start) caused sequential decreases in resistivity of up to approximately 30%. The addition of P (orange) and Rhodamine-WT (Rh-WT, pink) tracers produced very slight reductions in resistivity. The addition of KCl (green) produced an additional change in resistivity of approximately 20%. No significant changes in resistivity were observed in the gravel beneath the infiltration plot.

which are conservative tracers that will not sorb strongly to soil particles. Those tracers were added late in the infiltration sequence at a time when conditions beneath the plot were expected to be closest to saturation and hence hydraulic conductivities closest to maximum. In contrast, P is likely to sorb to fine-grained soil and thus not likely to be detected in MW samples. Likewise, the volume of infiltrating water itself is unlikely to be detected in the MWs as a rise in the water table in a coarse gravel aquifer.

The Cl⁻ concentrations in MW samples increased above background only in MW-A and MW-B (Fig. 6). The increase in MW-A appears in the sample taken 12 h after the Cl⁻ tracer was introduced to the plot and represents about 25% of the plot concentration. The increase in MW-B appears in the sample taken

25 h after introduction of the Cl⁻ tracer and represents only about 10% of the plot concentration. These MWs are located 1 m from the plot, with MW-A positioned downgradient and MW-B positioned parallel to the plot relative to the presumed GW flow direction. The low Cl⁻ concentrations in these wells coupled with the non-detect in the remaining wells implies that the bulk of the infiltration did not proceed vertically from the plot through the gravel vadose zone and into the alluvial aquifer where it could be sampled from MWs. Infiltration and fluid movement thus probably moved to areas not sampled by these conventional wells.

The temporal ERI images imply that the gravel–soil interface was behaving as a capillary barrier in the region directly below the plot. Two orthogonal temporal ERI data sets support a lack of
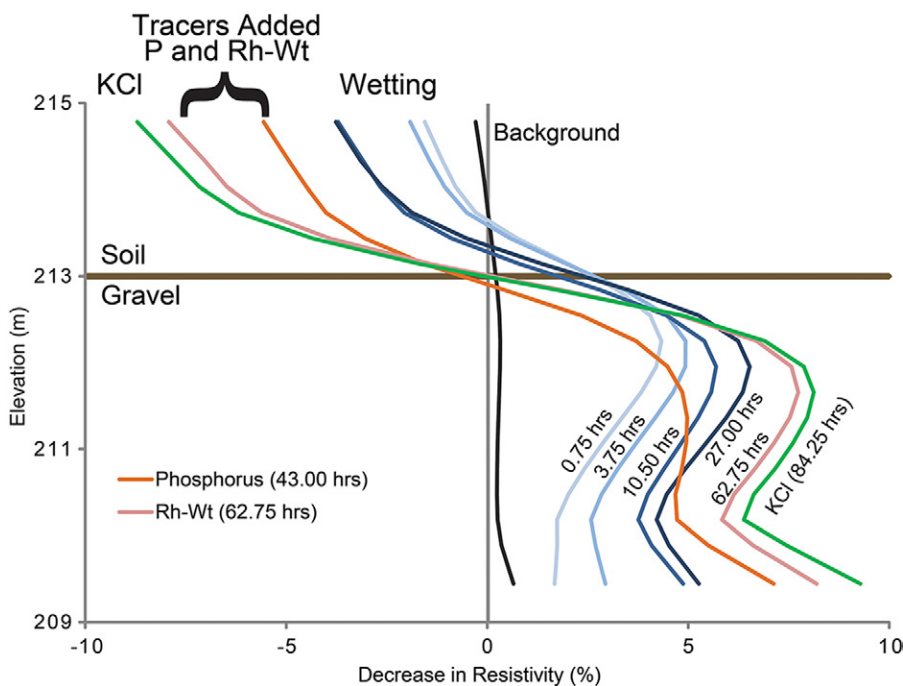

Fig. 9. Plot of the resistivity changes with elevation over time on line EW-2 at a location five m downgradient of the infiltration plot near monitoring well MW-G. The resistivity changes in the soil layer indicate increased resistivity, which was probably due to soil drying. Changes during the course of the infiltration experiment were <10%, which is similar to the minimal changes within the gravel layer shown in the lower portion of Fig. 7B.

infiltration into the gravel directly beneath the plot, but two additional temporal ERI datasets indicate the presence of vadose zone fluids in the gravel at distances of 5 m laterally from the plot. Flow paths can be drawn between the infiltration plot, downward to the gravel interface and over to the conductors on the adjacent lines 5 m away from the infiltration plot (Fig. 3 and 7). At the distal locations, the changes in conductance are largely beneath the gravel interface and are interpreted as breakthrough of fluids through the interpreted capillary barrier (Fig. 7 and 9). One flow path extends from the plot to the southwest and directs flow through the vadose zone nearly parallel to the presumed groundwater flow path. This direction is also parallel to a preferential flow path demonstrated by Heeren et al. (2011). The other flow path extends from the plot to the northwest and directs water and solutes through the vadose zone directly toward the stream. Because ERI lines were not positioned to the north and east, this experiment does not rule out the presence of other lateral flow paths.

The results of this field test are similar to those from laboratory tests of artificial capillary barriers (Stormont, 1996; Stormont and Anderson, 1999) and numerically modeled sand and gravel barriers (Ho and Webb, 1998) and show that naturally occurring pore-size contrasts can produce lateral diversion and unpredictable vadose zone flow paths. Additionally, the high data density of the ERI allowed tracking of flow paths through vadose zone soils and gravels in a way not possible with MWs or other conventional techniques. Further refinement of dynamic sampling of pathways focused on the capillary barrier zone and soil cores obtained at potential flow areas instead of reliance on MWs can improve the understanding of flow paths in these systems.

The overall goal for the research of tracking an infiltrated tracer into a highly heterogeneous gravel aquifer by sampling with wells was not obtained. The hypothesis that integrating MW data with geophysical data including targeted well sampling based on geophysical data to track fluids would allow us to catch isolated flow paths may still be a valid approach for systems without a capillary barrier in the vadose zone. The transient effects of the capillary barrier, which occurred in the context of steady infiltration, did not allow a regular flow path to develop during the experiment. A number of infiltration or tracer experiments have been conducted that have never observed the solute in MWs. This experiment is largely identical in the MW dataset. However, the geophysical data point to the cause of the lack of observed tracer in the MWs and thus point to alternative approaches that can be used in the future.

The dynamic sampling protocol that resulted in MW-G being installed after the initial temporal data collection assumed that once the flow path toward the MW-G location was established during infiltration, it would remain until infiltration ceased. The unsteady nature of flow along the capillary barrier violated that assumption. The location at MW-G did not continue to see increases in ERI conductance and appears, based on the existing data, to have had an increase in moisture content during the early part of the tracer experiment but did not result in a flow path that provided groundwater to the phreatic zone at MW-G. Coring at

that location or installation of a tensiometer may have been more effective at detecting tracer that migrated to the MW-G location. Having a black light or spectrophotometer onsite while coring would also be advantageous.

In building protocols for future tracer experiments, integrating geophysical data with well data will be useful but must be augmented with core data or tensiometer data from locations determined after processing the geophysical data. This will allow confirmation of the location and concentration of solute that entered the vadose zone but did not remain on a flow path for a duration that allowed migration to the phreatic zone and to a well. These experiments will be challenging but useful to demonstrate the transient controls on the spreading of solute through the vadose zone prior to solute ever entering the phreatic system. The protocols should allow for additional tracking through isolated heterogeneities once the solute makes it to the phreatic zone.

Conclusion

This study utilized seven monitoring wells, placed around a 1- by 1-m infiltration plot and along the presumed groundwater gradient and two orthogonal ERI arrays consisting of parallel lines to monitor the infiltration plot, which was constructed on a floodplain consisting of 1-m-thick silt loam topsoil overlying 2-m-thick subsurface gravel. During an 84.75-h constant infiltration period, solutes were sequentially added with known concentrations of P, Rh-WT, and Cl^-. Samples drawn from the monitoring wells showed only a minor amount of transport of the solutes from the plot to the groundwater table immediately surrounding the infiltration plot. However, ERI monitoring showed that the interface between the fine-grained soil and the coarse gravel acted as a capillary barrier, which prevented infiltration into the gravel beneath the plot. Differencing of sequential images for the parallel ERI lines showed that water and solute moved away from the plot in the vadose zone in at least two directions: to the southwest along a known flow path within the gravel vadose zone, and northwest directly toward the stream. Neither of these vadose zone flow paths directly intersected a MW, which is why ERI was more effective than MWs at characterizing the movement of the infiltrated water. While the experiment did not succeed in delineating transport into a highly heterogeneous gravel with a protocol that was designed to look for isolated flow paths, it was successful at indicating that the transient nature of capillary barriers that solute must pass through can control flow and transport prior to solute entering an isolated phreatic flow path.

References

Acharya, B.S., T. Halihan, C.B. Zou, and R.E. Will. 2017. Vegetation controls on the spatio-temporal heterogeneity of deep moisture in the unsaturated zone: A hydrogeophysical evaluation. Sci. Rep. 7:1499. doi:10.1038/s41598-017-01662-y

APHA. 1999. Method 4500-P J: Persulfate method for simultaneous determination of total nitrogen and total phosphorus. APHA, Washington, DC.

Andrews, W.J., M.F. Becker, S.J. Smith, and R.L. Tortorelli. 2009. Summary of surface-water quality data from the Illinois River basin in northeast Oklahoma, 1970–2007. Sci. Invest. Rep. 2009-5182. USGS, Reston, VA.

Arora, T., and S. Ahmed. 2011. Characterization of recharge through complex vadose zone of a granitic aquifer by time-lapse electrical resistivity tomography. J. Appl. Geophys. 73:35–44. doi:10.1016/j.jappgeo.2010.11.003

Beresnev, I.A., C.E. Hruby, and C.A. Davis. 2002. The use of multi-electrode resistivity imaging in gravel prospecting. J. Appl. Geophys. 49:245–254. doi:10.1016/S0926-9851(02)00147-7

Cassiani, G., A. Binley, and T.P.A. Ferré. 2006. Unsaturated zone processes. NATO Sci. Ser. 71:75–116. doi:10.1007/978-1-4020-4912-5_4

Corey, A.T. 1994. Mechanics of immiscible fluids in porous media. Rev. ed. Water Resour. Publ., Highland Park, CO.

Daniel, T.C., A.N. Sharpley, and J.L. Lemunyon. 1998. Agricultural phosphorus and eutrophication. A symposium overview. J. Environ. Qual. 27:251–257. doi:10.2134/jeq1998.00472425002700020002x

deGroot-Hedlin, C., and S. Constable. 1990. Occam's inversion to generate smooth, two-dimensional models from magnetotelluric data. Geophysics 55:1613–1624. doi:10.1190/1.1442813

Fox, G.A., D.M. Heeren, R.B. Miller, A.R. Mittelstet, and D.E. Storm. 2011. Flow and transport experiments for a streambank seep originating from a preferential flow pathway. J. Hydrol. 403:360–366. doi:10.1016/j.jhydrol.2011.04.014

Freiberger, R.P. 2014. Single- and dual-porosity calibration and long-term modeling of highly conductive floodplain soils in the Ozark ecoregion. M.S. thesis. Dep. of Biological Systems Engineering, Univ. of Nebraska, Lincoln, NE.

Fuchs, J.W., G.A. Fox, D.E. Storm, C.J. Penn, and G.O. Brown. 2009. Subsurface transport of phosphorus in riparian floodplains: Influence of preferential flow paths. J. Environ. Qual. 38:473–484. doi:10.2134/jeq2008.0201

Garabedian, S.P., D.R. LeBlanc, L.W. Gelhar, and M.A. Celia. 1991. Large-scale natural gradient tracer test in sand and gravel, Cape Cod, Massachusetts: 2. Analysis of spatial moments for a nonreactive tracer. Water Resour. Res. 27:911–924. doi:10.1029/91WR00242

Halihan, T., J. Albano, S.D. Comfort, and V.A. Zlotnik. 2011. Electrical resistivity imaging of a permanganate injection during in situ treatment of RDX-contaminated ground water. Groundwater Monit. Rem. 32:43–52. doi:10.1111/j.1745-6592.2011.01361.x

Halihan, T., and T. Fenstemaker. 2004. Proprietary electrical resistivity imaging method. 2nd ed. Oklahoma State Univ. Office of Intellectual Property, Stillwater.

Halihan, T., S.W. McDonald, P. Patey, and M. Stonecipher. 2012. ERI evaluation of injectates used at a dry-cleaning site. Remediation 22:79–91. doi:10.1002/rem.21322

Halihan, T., S. Paxton, I. Graham, T. Fenstemaker, and M. Riley. 2005. Post-remediation evaluation of a LNAPL site using electrical resistivity imaging. J. Environ. Monit. 7:283–287. doi:10.1039/b416484a

Halihan, T., V. Sefa, T. Sale, and M. Lyverse. 2017. Mechanism for detecting NAPL using electrical resistivity imaging. J. Contam. Hydrol. 205:57–69. doi:10.1016/j.jconhyd.2017.08.007

Heeren, D.M., G.A. Fox, A.K. Fox, D.E. Storm, R.B. Miller, and A.R. Mittelstet. 2014a. Divergence and flow direction as indicators of subsurface heterogeneity and stage-dependent storage in alluvial floodplains. Hydrol. Processes 28:1307–1317. doi:10.1002/hyp.9674

Heeren, D.M., G.A. Fox, R.B. Miller, D.E. Storm, A.R. Mittelstet, A.K. Fox, et al. 2011. Stage-dependent transient storage of phosphorus in alluvial floodplains. Hydrol. Processes 25:3230–3243. doi:10.1002/hyp.8054

Heeren, D., G. Fox, and D. Storm. 2014b. Berm method for quantification of infiltration at the plot scale in high conductivity soils. J. Hydrol. Eng. 19:457–461. doi:10.1061/(ASCE)HE.1943-5584.0000802

Heilig, A., T.S. Steenhuis, M.T. Walter, and S.J. Herbert 2003. Funneled flow mechanisms in layered soil: Field investigations. J. Hydrol. 279:210–223.

Hillel, D. 1987. Unstable flow in layered soils: A review. Hydrol. Processes 1:143–147. doi:10.1002/hyp.3360010203

Ho, C.K., and S.W. Webb. 1998. Capillary barrier performance in heterogeneous porous media. Water Resour. Res. 34:603–609. doi:10.1029/98WR00217

Khire, M., C. Benson, and P. Bosscher. 2000. Capillary barriers: Design variables and water balance. J. Geotech. Geoenviron. Eng. 126:695–708. doi:10.1061/(ASCE)1090-0241(2000)126:8(695)

LeBlanc, D.R., S.P. Garabedian, K.M. Hess, L.W. Gelhar, R.D. Quadri, K.G. Stollenwerk, and W.W. Wood. 1991. Large-scale natural gradient tracer test in sand and gravel, Cape Cod, Massachusetts: 1. Experimental design and observed tracer movement. Water Resour. Res. 27:895–910. doi:10.1029/91WR00241

Midgley, T.L., G.A. Fox, and D.M. Heeren. 2012. Evaluation of the bank stability and toe erosion model (BSTEM) for predicting lateral retreat on composite streambanks. Geomorphology 145–146:107–114. doi:10.1016/j.geomorph.2011.12.044

Miller, R.B., D.M. Heeren, G.A. Fox, T. Halihan, and D.E. Storm. 2015. Heterogeneity influences on stream water–groundwater interactions in a gravel-dominated floodplain. Hydrol. Sci. J. 61:741–750. doi:10.1080/02626667.2014.992790

Miller, R.B., D.M. Heeren, G.A. Fox, T. Halihan, D.E. Storm, and A.R. Mittelstet. 2014. The hydraulic conductivity structure of gravel-dominated vadose zones within alluvial floodplains. J. Hydrol. 513:229–240. doi:10.1016/j.jhydrol.2014.03.046

Miller, R.B., D.M. Heeren, G.A. Fox, D.E. Storm, and T. Halihan. 2011. Design and application of a direct-push vadose zone gravel permeameter. Groundwater 49:920–925. doi:10.1111/j.1745-6584.2010.00796.x

Moore, P.A., and D.R. Edwards. 2007. Long-term effects of poultry litter, alum-treated litter, and ammonium nitrate on phosphorus availability in soils. J. Environ. Qual. 36:163–174. doi:10.2134/jeq2006.0009

Murphy, J., and J.P. Riley. 1962. A modified single solution method for the determination of phosphate in natural waters. Anal. Chim. Acta 27:31–36. doi:10.1016/S0003-2670(00)88444-5

National Agriculture Imagery Program. 2010. 2010 Cherokee County, OK. [Shapefile.] USDA Farm Serv. Agency, Washington, DC.

Oklahoma Mesonet. 2013. Rainfall by month, Tahlequah, OK. Volume 2013. Oklahoma Climatol. Surv., Norman.

Opperman, J.J., G.E. Galloway, J. Fargione, J.F. Mount, B.D. Richter, and S. Secchi. 2009. Sustainable floodplains through large-scale reconnection to rivers. Science 326:1487–1488. doi:10.1126/science.1178256

Sima, A. 2008. Transient electrical resistivity imaging of a tracer test, Tahlequah, OK. M.S. thesis. Oklahoma State Univ., Stillwater.

Soerens, T.S., E.H. Fite III, and J. Hipp. 2003. Water quality in the Illinois River: Conflict and cooperation between Oklahoma and Arkansas. In: M. Bruen, editor, Proceedings of the 7th IWA International Specialised Conference on Diffuse Pollution and Basin Management, Dublin, Ireland. 17–21 Aug. 2003. University College, Dublin. p. 9-14–9-17.

Stormont, J.C. 1996. The effectiveness of two capillary barriers on a 10% slope. Geotech. Geol. Eng. 14:243–267. doi:10.1007/BF00421943

Stormont, J.C., and C.E. Anderson. 1999. Capillary barrier effect from underlying coarser soil layer. J. Geotech. Geoenviron. Eng. 125:641–648. doi:10.1061/(ASCE)1090-0241(1999)125:8(641)

Thorne, C.R., and N.K. Tovey. 1981. Stability of composite river banks. Earth Surf. Processes 6:469–484. doi:10.1002/esp.3290060507

USEPA. 1971. Method 365.2: Phosphorus, all forms (colorimetric, ascorbic acid, single reagent). USEPA, Environ. Monit. Syst. Lab., Cincinnati, OH.

USGS. 2013. USGS 07197000 Baron Fork at Eldon, OK. [Database.] USGS Natl. Water Inf. Syst., Reston, VA.

Werth, C.J., C. Zhang, M.L. Brusseau, M. Oostrom, and T. Baumann. 2010. A review of non-invasive imaging methods and applications in contaminant hydrogeology research. J. Contam. Hydrol. 113:1–24. doi:10.1016/j.jconhyd.2010.01.001